Available online at www.sciencedirect.com
SCIENCE DIRECT®
Journal of Magnetic Resonance 166 (2004) 111–122
JMR Journal of Magnetic Resonance
www.elsevier.com/locate/jmr

Equi-ripple design of quadratic-phase RF pulses

Rolf F. Schulte, Jeffrey Tsao, Peter Boesiger, and Klaas P. Pruessmann*

Institute for Biomedical Engineering, University and Swiss Federal Institute of Technology Zurich, Gloriastr. 35, 8092 Zurich, Switzerland

Received 18 June 2003; revised 7 October 2003

Abstract

An improved strategy for the design of quadratic-phase RF pulses with high selectivity and broad bandwidths using the Shinnar–Le Roux (SLR) transformation is proposed. Unlike previous implementations, the required quadratic-phase finite impulse response (FIR) filters are generated using the complex Remez exchange algorithm, which ensures an equi-ripple deviation from the ideal response function. It is argued analytically that quadratic-phase pulses are near-optimal in terms of minimising the B_1-amplitude for a given bandwidth and flip angle. Furthermore, several parameter relations are derived, providing practical design guidelines. The effectiveness of the proposed design method is demonstrated by examples of excitation and saturation pulses applied in vitro and in vivo.

Keywords: Quadratic phase pulses; Shinnar–Le Roux transformation; Broad bandwidth; Very selective saturation pulses; Frequency modulation

1. Introduction

Most magnetic resonance imaging (MRI) methods rely on frequency selective radio-frequency (RF) pulses, which become spatially selective with the application of magnetic field gradients. The quality and usefulness of such pulses is determined by several criteria, including the excitation profile, the maximum RF field strength $B_{1\max}$, the deposited energy and the length of the pulse. The ideal slice profile is a rectangular function for high selectivity. In other words, the excitation should be uniform within a chosen region and negligible outside this region. Furthermore, a broad excitation bandwidth is desired to reduce problems like the chemical shift displacement or the sensitivity to B_0 inhomogeneities.

In general, trade-offs have to be made among the various criteria mentioned above in order to obtain practically useful pulses. For common linear-phase pulses, which are essentially sinc-pulses, high selectivity requires a long pulse duration with many side lobes. For a broad excitation bandwidth, pulses of this type require high maximum RF field strength $B_{1\max}$, which is ultimately limited by the RF amplifier. For example, a typical limit for the B_1 amplitude is about 10 μT on a whole-body MRI scanner. At this RF field strength, linear-phase pulses achieve about 1 kHz for a 90° flip angle and 500 Hz for 180°. However, much larger bandwidths are required for many applications, especially at higher B_0 field strengths. As shown in [1–3], overlaying RF pulses with a quadratic phase in the frequency domain results in the RF energy of the main lobe being distributed more evenly over the pulse. Hence, for a given $B_{1\max}$ restriction, it is possible to achieve a broader bandwidth and improved selectivity by using quadratic-phase pulses.

However, the quadratic phase of these pulses limits their application as general pulses, since they cannot be refocused through linear gradients. Therefore, these pulses are most useful for purposes that do not require refocusing, such as the saturation and inversion of magnetisation. For these purposes, the phase distribution is irrelevant, while high selectivity, good agreement with the target profile and broad bandwidth remain essential. For instance, good outer volume suppression enables scanning with a reduced field of view and therewith reduced scan time in imaging [2]. Furthermore, the chemical shift displacement in PRESS can be reduced by saturating the region of displacement [4].

* Corresponding author. Fax: +41-1-632-1302.
E-mail address: pruessmann@biomed.ee.ethz.ch (K.P. Pruessmann).

1090-7807/$ - see front matter © 2003 Elsevier Inc. All rights reserved.
doi:10.1016/j.jmr.2003.10.009

A straightforward way of obtaining pulses with an approximately quadratic phase is to rescale adiabatic full passage pulses with offset independent adiabaticity [5]. However, pulses with improved characteristics, such as higher selectivity or error functions with constant error ripples, can be obtained by designing them from scratch. De novo design of RF pulses amounts to inverting the Bloch equations. This is particularly convenient in the small-tip-angle approximation [6], where the RF wave form and the pulse response can be approximated by a Fourier pair. For the design of pulses with large flip angles, several methods of non-linear optimisation have been proposed, using for instance optimal control theory [7,8] and simulated annealing [9].

An elegant and more analytical approach is the Shinnar–Le Roux (SLR) transformation [10,11], which reversibly transforms RF pulses into two complex finite impulse response (FIR) filters. The frequency response of these filters corresponds closely with the excitation profile of the RF pulse. Hence, the problem of RF pulse design reduces to that of designing low pass FIR filters. In case of linear-phase filters, this is a standard procedure for which many methods exist. The SLR transform is frequently used to design linear-phase pulses, which are purely amplitude-modulated. Nevertheless, the SLR concept is equally applicable for the design of RF pulses with frequency modulation, such as quadratic-phase pulses. However, FIR filters with a quadratic phase are more intricate to design.

FIR filters are represented in the z-transform domain as finite-order polynomial functions of a complex variable (z). Quadratic phase requires complex polynomial coefficients, which are generally more difficult to determine than real-valued coefficients for linear-phase pulses due to increased algebraic complexity and possible ill-conditioning of the problem [12,13]. A simple solution is to determine real and imaginary parts of the coefficients independently as though they were real-valued coefficients. This simplifies the problem, but does not generally yield the optimal solution [12].

Two methods have been previously proposed for determining the complex coefficients of approximately quadratic-phase FIR filters. The first one commences by designing a minimum-phase FIR filter with the desired magnitude response, whose phase pattern is then modified by root inversion [14]. The maximum frequency bandwidth achievable with this method is small due to numerical constraints and imprecise phase approximations. The second method is to calculate the polynomial coefficients of the desired FIR filter through a complex least-squares algorithm [2]. This optimisation minimises the deviation from the ideal response in terms of the 2-norm, which typically results in error overshoots at the band edges. A more favourable solution is the equi-ripple solution, where all error ripples are minimised to achieve equal magnitude. This is obtained by minimising the ∞-norm (Chebyshev norm) of the error function. An approximately equi-ripple error can also be obtained by introducing a proper weighting function in the least-squares optimisation. The implementation of this approach, as described in [2], performs a weighted least-squares fit to a pre-tailored target profile. With this method, the authors obtained an almost equi-ripple solution with broad bandwidth and high selectivity. Nevertheless, they report restrictions to the range of feasible quadratic-phase patterns.

In this work, we propose to obtain the equi-ripple solution directly, using the complex Remez exchange algorithm [12,13]. This permits determining quadratic-phase pulses with a wide range of quadraticity from zero (linear-phase) up to a critical maximum value. In the first part of the paper, the motivation for quadratic phase is reviewed. A simple heuristic reasoning is followed by a mathematical argument, which illustrates the near-optimality of quadratic-phase pulses in terms of minimising $B_{1\max}$. Then several parameter relations are described, providing design guidelines and illustrating trade-offs among the various pulse properties. In the subsequent sections, the actual design algorithms are described and validated by both simulations and MR experiments.

2. Motivation for quadratic-phase pulses

The advantage of quadratic-phase pulses can be appreciated by comparing them to linear-phase pulses. Most of the magnetisation in the selected band is rotated simultaneously with a linear-phase pulse. This requires a short main lobe, as its width is inversely-proportional to the bandwidth. The maximum B_1-amplitude of such pulses increases with the bandwidth, as the integral underneath the main lobe remains approximately constant for a given flip angle. Therefore, the $B_{1\max}$ and power limitations of the transmit coil and the RF amplifier restrict the bandwidth achievable with linear-phase pulses.

The key idea for reducing RF peak power is to excite the spins successively at their individual frequencies rather than all at once [14]. By sweeping through the desired frequencies sequentially, the pulse energy does not need to be confined to a single main lobe. Thus, the maximum RF amplitude can be significantly reduced. The most straightforward option, a linear frequency sweep, corresponds to multiplying the pulse envelope with a quadratic phase term. Interestingly, such a modulation also results in an approximately quadratic phase pattern in the spectral response of the pulse. Thus, the quadratic-phase response forms a suitable design goal for RF pulses with reduced peak power, enabling higher bandwidths. However, simply combining a linear frequency sweep with constant RF amplitude, forming a

so-called chirp pulse, results in a poor excitation profile. Thus, more sophistication is needed to combine a quadratic phase response with a proper rectangular amplitude profile.

The motivation for quadratic-phase pulses can also be argued from a more mathematical perspective, employing the Fourier transformation (FT), which approximates the solution of the Bloch equation for pulses with small flip angles [6]. This approximation holds strictly only for pulses with small flip angles θ with $\sin\theta \approx \theta$, but it holds sufficiently well to qualitatively describe the behaviour of pulses with a flip angle of up to about 90°.

The ideal excitation profile $|F(\omega)|$ is rectangular

$$|F(\omega)| = \mathrm{rect}(\omega), \quad \text{where}$$
$$\mathrm{rect}(\omega) = \begin{cases} 0, & \text{for } |\omega| > \mathrm{BW}/2, \\ \sin\theta, & \text{for } |\omega| \leqslant \mathrm{BW}/2, \end{cases} \tag{1}$$

where ω denotes the frequency, BW the bandwidth and θ the flip angle. If $F(\omega)$ has a linear phase, the RF wave form $f(t) = \mathscr{F}(F(\omega))$ is a sinc-function with a sharp peak and a large number of significant side lobes. Here, $\mathscr{F}()$ denotes the Fourier transform. In contrast, for efficient RF energy transfer in a limited time, the envelope $f(t)$ should ideally be rectangular as well. That is, the pulse envelope should be approximately rectangular in both the time and the frequency domain. These two seemingly conflicting requirements can be fulfilled only with a quadratic phase, as shown by Papoulis [15].

A rectangular function with an overlaid quadratic phase can be written as

$$f(t) = \frac{1}{\sqrt{-4\pi k i}}\ \mathrm{rect}\left(\frac{t}{2k}\right) \mathrm{e}^{-(\mathrm{i}t^2/4k)}, \tag{2}$$

where k is a scaling constant and rect is defined as in Eq. (1). Eq. (2) is expressed in the frequency domain as

$$F(\omega) = \frac{1}{\sqrt{-4\pi k i}} \cdot \mathscr{F}\left(\mathrm{rect}\left(\frac{t}{2k}\right)\right) \otimes \mathscr{F}\left(\mathrm{e}^{-(\mathrm{i}t^2/4k)}\right). \tag{3}$$

The convolution in Eq. (3) can be developed into an asymptotic series, as shown in [15]. For a sufficiently large k and a sufficiently smooth envelope, this series can be approximated by

$$F(\omega) \approx \mathrm{e}^{\mathrm{i}k\omega^2}\mathrm{rect}(\omega). \tag{4}$$

In this expression, k specifies the amount of quadratic phase applied in the frequency domain. Generally, the Fourier transform of a smooth envelope function with a quadratic phase yields the same envelope in the other domain, again with a quadratic phase. In the desired rectangular profile, the smoothness criterion is violated at the two discontinuities. As a consequence, the ideally rectangular envelope in the time domain will deteriorate at its edges. Incidentally, by swapping t and ω, the same reasoning explains why chirp pulses, which have the ideal rectangular profile in the time domain, have such poor excitation profiles.

According to Parseval's theorem

$$\|f(t)\|_2 = \sqrt{\int_{-\infty}^{\infty} |f(t)|^2 \,\mathrm{d}t} = \frac{\|F(\omega)\|_2}{2\pi} \propto \sqrt{\mathrm{BW}}\,\sin\theta. \tag{5}$$

Hence, the 2-norm is fixed for a given bandwidth BW and flip angle θ. In turn, for a fixed norm and pulse duration, the smallest peak amplitude is achieved by a pulse with a constant envelope (i.e., $|f(t)| = \mathrm{const}$), which is accomplished precisely with quadratic phase in the limit of large k. In other words, practical quadratic-phase pulses are almost optimal in terms of minimising the peak RF amplitude for a given pulse duration, bandwidth, and flip angle.

3. Parameter definitions and relations

Successful design of quadratic-phase pulses that match the target specifications closely requires trade-offs among the design parameters. The main parameters include the bandwidth

$$\mathrm{BW} = \frac{\omega_\mathrm{s} + \omega_\mathrm{p}}{2}, \tag{6}$$

and the fractional transition width

$$\mathrm{FTW} = \frac{\omega_\mathrm{s} - \omega_\mathrm{p}}{\mathrm{BW}}, \tag{7}$$

which is a relative expression for the selectivity. ω_s and ω_p are the stop and pass band frequencies. Further key parameters are the flip angle θ, the filter length n and the amount of quadratic phase k. The parameter settings lead to certain pulse properties, such as the maximum RF amplitude $B_{1\,\mathrm{max}}$, the energy of the pulse and the resulting error function, which is defined as the deviation from the target profile. In the following, several relationships among pulse parameters and properties are established as design guidelines.

To clarify the subsequent description, it is important to distinguish between normalised and physical quantities. In FIR filter design, the frequency ω is usually normalised to the range $[-\pi, \pi]$. The inverse SLR transformation can be used to convert such filters into an RF pulse shape with normalised time, whose duration is equal to the filter length n. This pulse can then be scaled to any physical duration, thus rescaling frequency and time to physical units. Throughout this paper, physical frequency and time will be distinguished from their normalised counterparts by the tilde symbol. The quantities in physical units are given by:

$$\tilde{\omega} = \frac{\omega}{\Delta\tilde{t}}, \tag{8}$$

$$\tilde{T} = n\Delta\tilde{t}, \tag{9}$$

$$\tilde{k} = k\Delta\tilde{t}^2, \tag{10}$$

$$\tilde{B}_1 = \frac{B_1}{\gamma\Delta\tilde{t}}, \tag{11}$$

where $\Delta\tilde{t}$ denotes the sample spacing, $\tilde{T}$ the total duration of the pulse and γ the gyromagnetic ratio. With these relationships it is straightforward to scale an RF pulse to different pulse durations.

3.1. Time-bandwidth product

The physical bandwidth of the RF pulse is given by

$$\widetilde{\mathrm{BW}} = \frac{\mathrm{BW}}{\Delta\tilde{t}}. \tag{12}$$

With Eq. (9) this leads to the time-bandwidth product of the RF pulse

$$\tilde{T}\,\widetilde{\mathrm{BW}} = n\,\mathrm{BW}, \tag{13}$$

which is invariant under time and frequency scaling and thus is a key characteristic of an RF pulse. This product is fundamentally limited by digitisation. For quadratic-phase pulses, an estimate of this limitation can be derived from Eqs. (2) and (4) for moderate flip angles. Ideally, the cutoff values of the rectangular functions in the two domains are related through $\omega = t/2k$, leading to

$$\mathrm{BW} = \frac{n}{2k}. \tag{14}$$

As mentioned, when enforcing a good rectangular shape in the frequency domain, the corresponding profile in the time domain will degrade at its edges and extend beyond the idealised pulse duration. In order to still capture the entire pulse, Eq. (14) must allow for some slack in the time domain. This results in

$$\mathrm{BW} \ll \frac{n}{2k}. \tag{15}$$

Combined with Eq. (13), this yields

$$\tilde{T}\widetilde{\mathrm{BW}} \ll \frac{n^2}{2k}. \tag{16}$$

That is, for achieving a high time-bandwidth product with a given k value, n must be sufficiently large. Note that k needs to be large as well in order to justify the series expansion underlying Eq. (4) and to reduce $B_{1\max}$, as discussed in the following.

3.2. Amount of quadratic phase

The amount of quadratic phase k is an important design parameter, which needs to be chosen carefully. The desired effect of the quadratic phase is to distribute the RF energy more evenly across the pulse duration, thus reducing $B_{1\max}$ as illustrated in Fig. 1. For small k-values, $B_{1\max}$ is not sufficiently reduced. On the other hand, there is also an upper limit for k, beyond which errors in the profile increase disproportionately. This limit for k is difficult to assess analytically, yet can be estimated as follows.

In the small-tip-angle approximation, the function $f(t)$ in Eq. (2) is equal to the RF field strength $B_1(t)$. For constant $|B_1|$ and sufficiently large k, the flip angle θ in the pass band can be derived from Eq. (2) through

$$\theta = |B_1|\sqrt{4\pi k}. \tag{17}$$

For a constant θ, this leads to the following proportionality:

$$k \propto \frac{1}{B_1^2}. \tag{18}$$

Thus, k must be large in order to reduce B_1 effectively. The product kB_1^2 stays approximately constant when varying the amount of quadratic phase, as illustrated in Fig. 2.

However, increasing value of k also leads to increased error of the pulse profile, as shown in Fig. 3. The error is defined here as the maximum deviation from the target profile. To account for undesired overshoots in the transition bands, values in the transition bands that exceed the target pass band value were rated as errors as well. The error for $k = 0$ (i.e., linear-phase pulses) is related to an empirically derived performance measure given by ($n\,\mathrm{BW}\,\mathrm{FTW}$) [10]. The increase of this error when applying quadratic phase can be best understood in connection with Eq. (15). When increasing k, the envelope in the time domain widens, as shown in Fig. 1. As the finite pulse length n remains the same, the be-

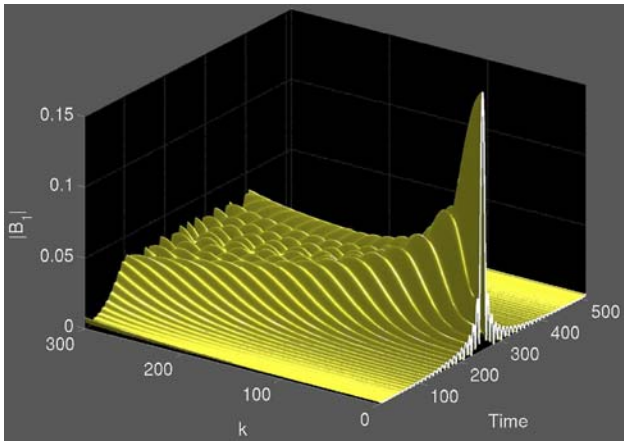

Fig. 1. Effect of different amounts of quadratic phase k on the magnitude of the RF pulse (Remez pulse with $n = 512$, $\theta = 90°$, $\omega_p = 0.1\pi$, and $\omega_s = 0.11\pi$). The pulse at $k = 0$ corresponds to a regular linear-phase pulse. For increasing k the RF energy is spread out further and further away from the original central main lobe.

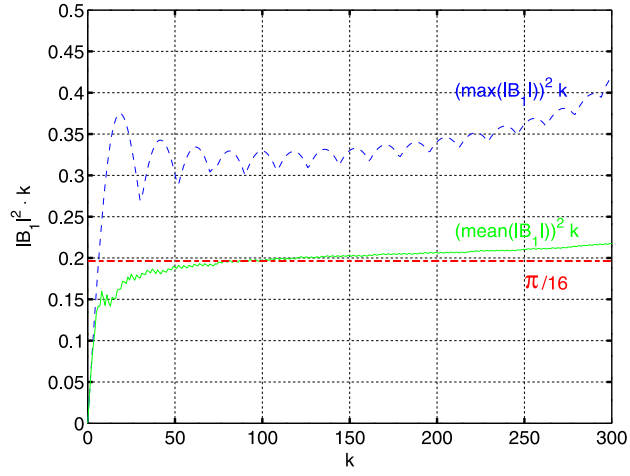

Fig. 2. The square of the B_1 amplitude of Fig. 1 times k is plotted against k, showing that Eq. (18) holds well in a wide range of k values. The dashed line denotes the maximum B_1 value, the solid line is the mean value over the bandwidth calculated through Eq. (14) and the default value from Eq. (17) $\pi/16$ with $\theta = \pi/2$ is plotted with a dash-dotted line.

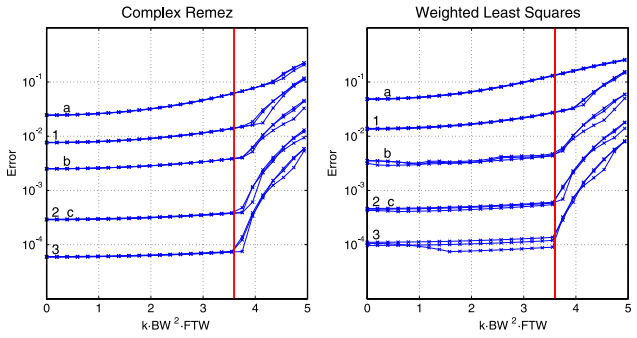

Fig. 3. The pulse design error as a function of the parameter setting (varying k, BW, FTW). The error plotted here is the maximum error ripple, including the ripple in the transition band exceeding the value of the pass band. In series a, b, and c, the fractional transition width is held constant (FTW = 0.1) and the bandwidth is varied (a, $BW \cdot n = 80.4$; b, $BW \cdot n = 160.8$; and c, $BW \cdot n = 241.3$). In the other series 1, 2, and 3, the bandwidth is held constant ($BW \cdot n = 241.3$), while the fractional transition width is varied (1, FTW = 0.05; 2, FTW = 0.1; and 3, FTW = 0.125). Each series contains three lines, corresponding to three different filter lengths ($n = 256$, $n = 512$, and $n = 1024$). Beyond a critical value of $k \cdot BW^2 \cdot FTW \approx 3.6$ (vertical line), the pulse design error increases sharply due to the emergence of an overshoot in the transition band.

ginning and the end of the idealised pulse become more and more truncated, leading to gradually increasing errors. Thus, k is ultimately limited by the pulse length, as previously observed in Eq. (15).

Another limitation to the degree of quadraticity was found empirically. As shown in Fig. 3, the maximum error in the fitted FIR filter grows slowly as a function of k for moderate k values. Yet, beyond some critical degree of quadraticity, the error tends to rise sharply. This effect is due to the onset of an overshoot in the

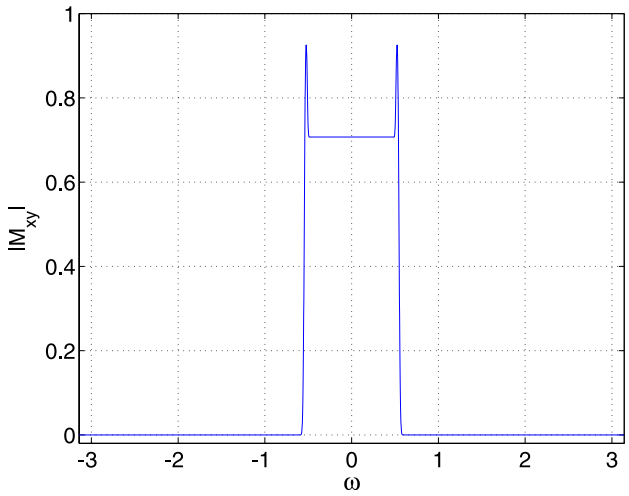

Fig. 4. Unfavourable parameter selection (i.e., too high ($k\,BW^2\,FTW$) product) can lead to high overshoots inside the transition band. As this band is not considered during the fitting procedure, one has to choose a different parameter set. Here: $k\,BW^2\,FTW = 14$.

transition band, as depicted in Fig. 4. As shown in Fig. 3, this overshoot tends to occur when the product $k\,BW^2\,FTW$ reaches a certain threshold, suggesting that k should generally fulfil

$$k \lesssim \frac{3.6}{BW^2\,FTW}. \tag{19}$$

The critical value of 3.6 is a rough guideline and subject to slight changes depending on the specific parameter configuration. In practice, a more precise maximum value for k is readily found by a few design iterations. The upper bound expressed in Eq. (19) tends to be more limiting than that expressed in Eq. (15). Generally, for robust quadratic-phase pulse design both inequalities should be fulfilled.

3.3. Filter length n

The number of samples n of the RF pulse is not ultimately significant [10], as long as n is large enough for the chosen time-bandwidth product and k value. Above a certain limit, a higher n while retaining the same time-bandwidth product and fractional transition width will only lead to a finer discretisation in the time domain, while leaving the error in the frequency response largely unaffected. On the other hand, insufficient n leads to a violation of Eq. (15) and thus an erroneous fit. Furthermore, the rotations represented in the individual segments of the pulse become larger as n decreases. This leads to an increasing violation of the hard pulse approximation, which underlies the SLR transformation. As a result, the actual frequency response of the RF pulse will deviate from the frequency response of the FIR filter. In these respects, choosing a large n is advisable, although excessive filter lengths n should be

avoided as they increase computation times and may lead to numerical instabilities.

3.4. Energy

In the context of in vivo application another main design restriction is the energy deposited by the RF pulse in the tissue. The energy deposited per unit time is commonly referred to as specific absorption rate (SAR), which is subject to rigid safety regulations. The pulse energy is proportional to the square of the 2-norm of $\tilde{B}_1$ [2], which in turn is proportional to $\widetilde{\mathbf{BW}}$ and θ^2 in the small-tip-angle regime (Eq. (5))

$$Q \propto \int_{-\tilde{T}/2}^{\tilde{T}/2} |\tilde{B}_1(\tilde{t})|^2 \, \mathrm{d}\tilde{t} \propto \widetilde{\mathbf{BW}}\, \theta^2. \tag{20}$$

Frequency modulation can be neglected here, as it is far lower than the precession frequency.

For low flip angles, the pulse energy Q depends solely on the flip angle and the bandwidth $\widetilde{\mathbf{BW}}$ as derived in Eq. (20). Thus, pulses with the same bandwidth and flip angle deposit the same energy [2]. In other words, quadratic-phase pulses behave like regular linear-phase pulses in this respect, at least in the small-tip-angle regime.

4. Methods

The SLR transformation converts the problem of inverting the Bloch equations into that of designing two complex polynomials $A(z)$ and $B(z)$, which represent regular FIR filters. Hence, it is possible to use the comprehensive methodology of FIR filter design for RF pulse design. $A(z)$ and $B(z)$ are $(n-1)$th order polynomials that represent the frequency-dependent Cayley–Klein parameters of the rotation effected by the corresponding RF pulse. For instance, the transverse magnetisation created by a pulse from initial z-magnetisation of M_0 is given by [10]

$$M_{xy} = 2A(z)^* B(z) M_0, \tag{21}$$

where the asterisk denotes complex conjugation and $z = \mathrm{e}^{\mathrm{i}\omega}$ is the argument of the polynomials. In the following, "$A(z)$" and "$B(z)$" will be used interchangeably with "$A(\omega)$" and "$B(\omega)$" for notational convenience. Since the Cayley–Klein polynomials represent rotations, they satisfy the following constraint:

$$A(z)A^*(z) + B(z)B^*(z) = 1, \tag{22}$$

for all values of z, which leads to

$$|M_{xy}(\omega)| = 2\sqrt{1 - |B(\omega)|^2} \cdot |B(\omega)| M_0. \tag{23}$$

Hence, if $|B(\omega)|$ describes a rectangular profile as a function of ω, the excited transverse magnetisation

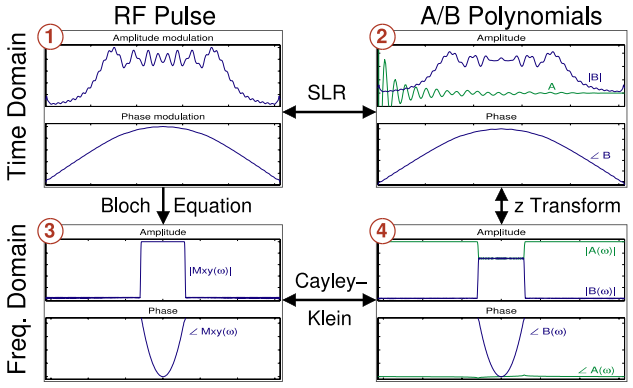

Fig. 5. The relationships between the different domains associated with the Shinnar–Le Roux (SLR) transform, shown for a typical quadratic-phase RF pulse. The SLR transform links the RF pulse (1) with an equivalent pair of FIR filters, A and B. The coefficient (2) and frequency (4) representations of these filters are connected by the z-transform. The frequency response of the FIR filters is related to the excitation profile of the RF pulse (3) by the Cayley–Klein rotational parameters. The excitation profile can equally be obtained by directly integrating the Bloch equations ($1 \Rightarrow 3$). However, in the reverse direction the direct pathway, i.e., Bloch inversion, is generally not available. Instead, SLR pulse design operates via the stages 4 and 2, exploiting the reversibility of the intermediate transforms.

$|M_{xy}(\omega)|$ will also exhibit a rectangular envelope. For the design of low pass pulses, it is thus possible to first design a suitable B polynomial and then generate a matching A polynomial that satisfies Eq. (22). Typically, and in the current work as well, the A polynomial is created through the Hilbert transform, leading to a minimum-phase frequency response of A, as described in [10]. When the phase of A is negligible, the phase of M_{xy} will be similar to that of the B polynomial. Therefore, an RF pulse with a quadratic-phase frequency response can be generated on the basis of a B FIR filter with a quadratic phase and a corresponding minimum-phase A polynomial. The relationship between the RF pulse and the A and B polynomials is depicted in Fig. 5.

In the following, two methods are described for creating FIR filters with complex coefficients. The first method is least-squares optimisation, which employs a weighting function for obtaining an approximately equi-ripple error function, as previously suggested in [2]. The second one is the proposed method, which uses the complex Remez exchange algorithm [12,13] to directly achieve a truly equi-ripple error function without the need for heuristic spectral weighting. This algorithm is a generalisation of the Remez/Parks–McClellan algorithm [16], which permits approximating arbitrary magnitude and phase response functions.

4.1. Target filter response

The desired frequency response, to which $B(\omega)$ will be fitted, is expressed as

$$D(\omega) = R(\omega)\mathrm{e}^{\mathrm{i}\varphi(\omega)}, \tag{24}$$

where $R(\omega)$ and $\varphi(\omega)$ are real-valued functions, describing the desired magnitude and phase responses, respectively. For a low pass quadratic-phase response, they are expressed as:

$$R(\omega) = \begin{cases} 0, & \text{for } |\omega| \geqslant \omega_\mathrm{s}, \\ \sin\left(\frac{\theta}{2}\right), & \text{for } |\omega| \leqslant \omega_\mathrm{p}, \end{cases} \qquad \varphi(\omega) = k\omega^2, \tag{25}$$

where θ is the desired flip angle and ω_p and ω_s are the pass and stop band frequencies. The gaps between the pass and the stop bands are referred to as the transition bands. The $\sin(\theta/2)$ originates from the SLR transformation and is derived from Eq. (23) by setting $|M_{xy}|$ to $(M_0 \sin\theta)$ for $0 \leqslant \theta \leqslant \pi$. It should be noted, that ω is the symmetric and normalised frequency in the range $[-\pi, \pi]$. In the literature, the range of ω is frequently defined as $[0, 2\pi]$ with a centre frequency of π. This only refers to a shift of reference, and in that case $\varphi(\omega)$ would include a linear phase term as well. Note also, that it is easily possible to extend this target to an asymmetric function, for instance to obtain one sharper side.

4.2. Error function

The FIR filter to be designed is a polynomial of the form

$$B(\omega) = \sum_{j=0}^{n-1} b_j \mathrm{e}^{-\mathrm{i}j\omega}, \tag{26}$$

where b_j denotes the complex jth polynomial coefficient. The difference between this filter and the desired response function $D(\omega)$ is expressed by the error function

$$E(\omega) = W(\omega)(D(\omega) - B(\omega)), \tag{27}$$

where $W(\omega)$ is a real and non-negative weighting function. In the transitions bands, $W(\omega)$ is generally set to zero.

4.3. Least-squares fit

As described in [2], a least-squares fit of the target filter response is obtained by minimising the 2-norm of the error function

$$\|E(\omega)\|_2 = \sqrt{\int_{-\pi}^{\pi} |E(\omega)|^2 \,\mathrm{d}\omega}. \tag{28}$$

With uniform error weighting this approach leads to overshoots at the band edges. However, the weighting function $W(\omega)$ can be adjusted to place more emphasis in these areas and thus reduce overshoots. A feasible weighting function for an approximately equi-ripple solution was found to be [2]

$$W(\omega) = \frac{1}{\delta(\omega)} \sqrt{1 + 10\left(\frac{1}{\left(\omega - \frac{1}{2}(\omega_\mathrm{s} + \omega_\mathrm{p})\right)^2} + \frac{1}{\left(\omega + \frac{1}{2}(\omega_\mathrm{s} + \omega_\mathrm{p})\right)^2}\right)}, \tag{29}$$

where $\delta(\omega) = \delta_1$ is the relative target ripple of the polynomial in the pass band, $\delta(\omega) = \delta_2$ in the stop band and $\delta(\omega) = \infty$ (i.e., $W(\omega) = 0$) in the transition band.

For numerical treatment, the normalised frequency ω must be discretised. An equi-distant discretisation of the frequency is given by

$$\omega_l = \Delta\omega\left(l + \frac{1}{2}\right) - \pi, \tag{30}$$

where $\Delta\omega = (2\pi)/m$ denotes the sampling frequency and the index l counts from 0 to $(m-1)$. The number of sampling points m needs to be much larger than the filter length n for sufficient accuracy.

Using this discretisation, the minimisation problem can be reformulated in terms of matrix notation. The actual and desired filter responses B and D, and the error function E are transformed into the vectors $\mathbf{B}$, $\mathbf{D}$, $\mathbf{E}$ by sampling along ω_l. By assembling the polynomial coefficients b_j from Eq. (26) in a similar fashion, the actual filter response can be expressed as

$$\mathbf{B} = \mathbf{U}\mathbf{b}, \tag{31}$$

where the entries of the $m \times n$ matrix $\mathbf{U}$ are given by

$$u_{l,j} = \mathrm{e}^{-\mathrm{i}j\omega_l}. \tag{32}$$

The weighting function from Eq. (29) can be incorporated as an $m \times m$ diagonal matrix $\mathbf{W}$, with its diagonal elements given by

$$w_{l,l} = W(\omega_l). \tag{33}$$

Hence, Eq. (27) can be restated as

$$\mathbf{E} = \mathbf{W}(\mathbf{D} - \mathbf{U}\mathbf{b}), \tag{34}$$

and the optimal coefficient vector $\mathbf{b}$ is characterised by a minimum of the 2-norm of $\mathbf{E}$. The minimum-norm solution can be calculated with the Moore–Penrose [17] pseudo-inverse (†)

$$\mathbf{b} = (\mathbf{W}\mathbf{U})^\dagger \mathbf{W}\mathbf{D}. \tag{35}$$

4.4. Complex Remez for Chebyshev-norm

In the proposed method, the truly equi-ripple solution is obtained by finding filter coefficients that minimise the Chebyshev (i.e., maximum) error norm

$$\|E(\omega)\|_\infty = \max_\omega\{|E(\omega)|\}, \tag{36}$$

with $E(\omega)$ defined as in Eq. (27). The major advantage of Chebyshev optimisation is that it does not require a particular weighting function for approximating equi-ripple

behaviour. It minimises the maximum error, which forces the magnitudes of the error ripples to be the same everywhere. Therefore, the weighting function $W(\omega)$ is now constant everywhere apart from the transition bands, which are exempt from optimisation. Nevertheless, one may also choose to apply different constant weights on the pass and stop bands in order to individually alter the magnitude of the error ripples in the different bands.

Chebyshev optimisation of FIR filters with complex coefficients can be accomplished with the complex Remez exchange algorithm. For a detailed description of the algorithm, the reader is referred to [12,13]. Briefly, to minimise the Chebyshev norm efficiently, the main strategy is to sample $E(\omega)$ only at a sparse, finite subset S of frequencies and iteratively adapt these frequencies such that they sample the extreme values of the error ripples. This basic approach consists of two steps, which are depicted on the right in Fig. 6. In a first step, the best approximation in terms of $\|E_S(\omega)\|_\infty$ (Eq. (36)) on the sparse subset is calculated. In a second step, this subset is altered such that the maximum error norm $\|E_S(\omega)\|_\infty$ of this subset increases. The optimal solution is found iteratively repeating both steps until the subsets remain the same.

The complex Remez algorithm (Fig. 6, top left) performs these steps with subsets of $n+1$ points, where n is the filter length. In this case, the minimisation problem on each subset reduces to a linear system of equations, which can be solved very efficiently. The optimal solution is found when the error norm on the subset, $\|E_S(\omega)\|_\infty$, converges toward the actual error norm on the continuous set, $\|E(\omega)\|_\infty$. This is generally the case

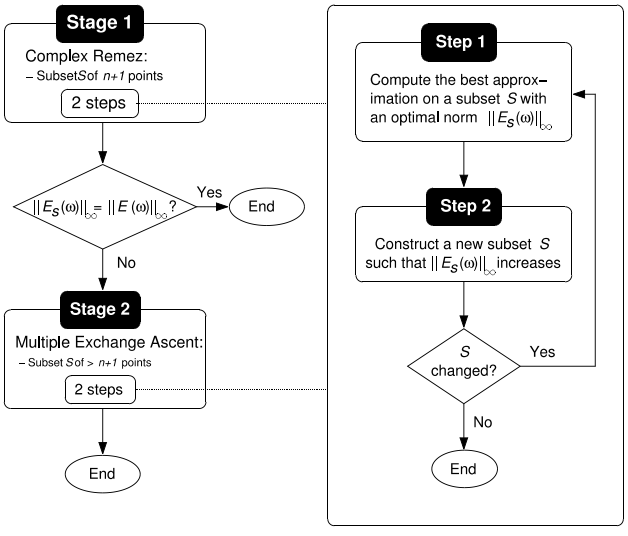

Fig. 6. Schematic of the algorithm for finding the optimal FIR filter $B(\omega)$. The solution is characterised by a minimum of the Chebyshev norm of the error function $E(\omega)$, corresponding to equi-ripple error. Two stages (left) iterate through a two-step process until the optimal solution is found. The second stage is invoked only if the first stage fails to converge.

for parameter sets that comply with the relations described in Section 3. For the case of non-convergence of the complex Remez algorithm, a more advanced method was described in [13]. This method, a generalised multiple-exchange ascent algorithm, forms the optional second stage of the optimisation procedure (Fig. 6, bottom left). It performs the same steps as described above, yet samples the error function more densely and uses a more intricate method for subset iteration. Using the result of the first stage as an initial estimate, the second stage converges safely, yet at the expense of drastically increased computation time. However, it was found empirically that the second algorithm needs to be invoked only in cases with unfavourable parameter relations. In these cases, even the optimal solution must typically be discarded due to high error levels. For the present work, the complex Remez and multiple-exchange ascent algorithms were performed under MATLAB (The MathWorks, Natick, MA, USA), using an implementation available in the signal processing toolbox.

4.5. Validation study

To validate the proposed methods, an exemplary RF pulse was designed with a time-bandwidth product of 330 (in radians), a fractional transition width of 0.073, a flip angle of $\theta = 90°$, $k = 120$, and $n = 512$ samples. For comparison, two pulses with the same specifications were additionally designed using the least-squares approach with either the weighting function given by Eq. (29) or constant weights.

The excitation profiles of these pulses were verified by numerical integration of the Bloch equations employing a fourth-order Runge–Kutta method [18]. Additionally, the pulses were verified experimentally on a Philips 1.5 T Intera whole-body MR scanner equipped with a transmit/receive birdcage resonator (Philips Medical Systems, Best, The Netherlands). Both excitation and saturation capabilities were shown on a phantom containing one litre of doped water solution ($T_1 = 360$ ms; $T_2 = 320$ ms). Furthermore, the saturation of magnetisation was demonstrated in vivo in an axial section through the human brain. Written informed consent was obtained from the healthy volunteer prior to imaging.

All experiments were based on regular spin echo imaging sequences. In the excitation experiments, the quadratic-phase RF pulse was used for 90° excitation, with a selection gradient in the same direction as the readout gradient. The 180° refocusing pulse was then used to select the image plane ($T_E = 40$ ms, $T_R = 800$ ms). In the saturation experiments, the quadratic-phase pulse was used for exciting the magnetisation, again in a perpendicular slice, followed by spoiler gradients and the full spin-echo sequence with normal slice selection ($T_E = 30$ ms, $T_R = 800$ ms).

5. Results

The amplitude and frequency modulation of the exemplary pulse (see Section 4.5) is shown in Fig. 7. For a duration of $\tilde{T} = 5\,\text{ms}$ it has a maximum RF field strength of $\tilde{B}_{1\,\max} = 20\,\mu\text{T}$. For comparison, the maximum RF field strength of a linear-phase pulse with the same specifications is more than threefold at $\tilde{B}_{1\,\max} = 68\,\mu\text{T}$. The complex Remez design is compared to the alternative design methods in Fig. 8. The upper row shows the magnitude of the deviation between the desired and the achieved profiles designed with the complex Remez, weighted least-squares and plain least-squares algorithms. These results illustrate that direct Chebyshev optimisation yields an exact equi-ripple error function, while some variation in the error level is obtained with either weighted or plain least-squares.

From the A and B polynomials, the transverse magnetisation was calculated through $M_{xy} = 2A^*BM_0$ and the longitudinal magnetisation through $M_z = (AA^* - BB^*)M_0$ [10], setting M_0 to one. In the middle and lower row of Fig. 8, the deviation of M_{xy} and M_z from their ideal profiles are plotted for the complex Remez, weighted least-squares and plain least-squares methods. The error level in M_{xy} and M_z is different between pass and stop bands, reflecting the non-linear relationship between $B(\omega)$ and the components of the magnetisation. This effect can be readily compensated for by appropriate weights applied to the pass and stop bands [10], as shown in Fig. 9.

In case of the complex Remez, the transverse magnetisation has a truly equi-ripple error function in the stop band. However, in the pass band, the error shows some modulation, falling below the equi-ripple level in small intervals. This is due to the fact that M_z and $|M_{xy}|$ depend only on the modulus of $B(\omega)$ (see Eq. (23)). As a consequence, only errors that are in phase with $B(\omega)$ do actually propagate into M_z and $|M_{xy}|$. Out-of-phase errors get masked, causing said incisions in the error plots. The same also applies to the least-squares methods, which additionally show variation in the error envelope. In case of weighted least-squares these variations have

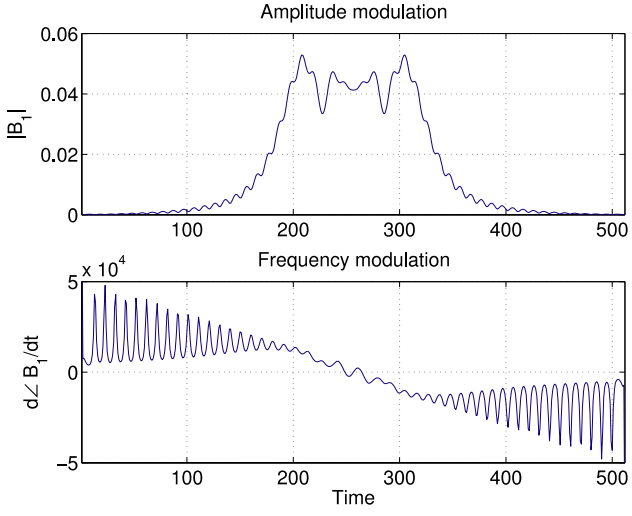

Fig. 7. Quadratic-phase pulse designed with the complex Remez exchange algorithm. The design parameters were: $n = 512$, $\theta = 90°$, $\omega_p = 0.095\pi$, $\omega_s = 0.11\pi$, and $k = 120$. This pulse was used for the validation study (Figs. 11 and 12).

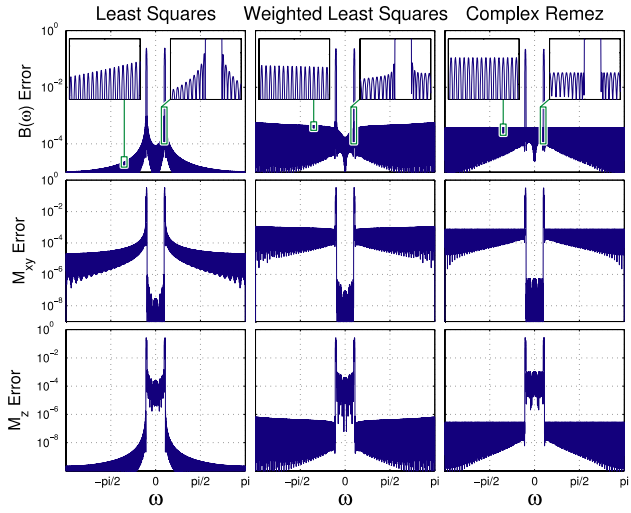

Fig. 8. Comparison of FIR filter design with least-squares (left), weighted-least-squares (middle), and complex Remez (right), based on the pulse specifications given in Fig. 7. The top row shows the error in the FIR filter response $|B(\omega) - D(\omega)|$. The structure of the error ripples is illustrated in the magnified insets. The two major peaks in each plot correspond to the transition bands and do not represent actual errors. Only the complex Remez algorithm yields error ripples of constant magnitude throughout the pass and stop bands. The middle and bottom rows show the resulting error in the transverse and longitudinal magnetisation, respectively. For the magnetisation the error levels differ between the pass and stop bands, reflecting the non-linear relationship between $B(\omega)$ and the components of the magnetisation (Eq. (23)).

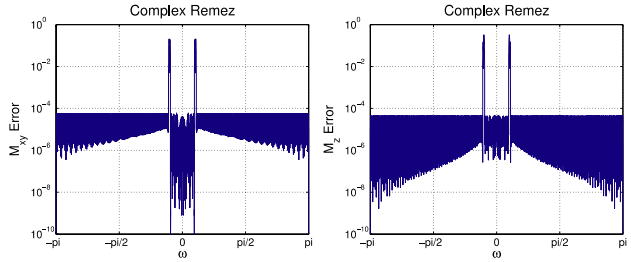

Fig. 9. Error in the transverse ($||M_{xy}| - |M_{xy}^{\text{ideal}}||$; left) and longitudinal ($|M_z - M_z^{\text{ideal}}|$; right) magnetisations, obtained with a quadratic-phase complex Remez pulse. The pulse specifications were the same as for Figs. 7 and 8. However, different error weighting was applied in the pass and stop bands to match the ripple magnitude in all three bands. For equi-ripple transverse magnetisation (left), the weight on the stop bands was exaggerated 140-fold. For equi-ripple longitudinal magnetisation (right), the weight on the pass band was exaggerated 300-fold.

been found to significantly depend on the chosen parameter settings, making it difficult to choose an optimal weighting function a priori. The plain least-squares fitting procedure with constant weighting is generally unfavourable as errors increase significantly near the transition band.

The effect of scaling $\tilde{B}_1$ to different flip angles is depicted in Fig. 10 for both transverse and longitudinal magnetisation. By rescaling the applied RF field, the bandwidth remains unchanged, but the profile deteriorates. Hence, for each target flip angle a specific RF pulse should be designed rather than rescaling an existing pulse.

The results of the experimental validation study are shown in Figs. 11 and 12. Fig. 11 shows the in vitro experiments on the phantom, for both excitation and saturation. Note the quadratic phase of the magnetisation, which is only slightly distorted by the minimum-phase $A(z)$ polynomial. When used for selective saturation, the designed pulse leaves only little magnetisation remaining. Fig. 12 demonstrates the selective saturation in vivo in the brain of a healthy human.

The complex Remez algorithm is relatively fast for properly chosen parameters. For instance, designing the RF pulse shown in Fig. 7 required 10 s on a current CPU (Intel Pentium 4, 2.53 GHz), running MATLAB 6.5 R13

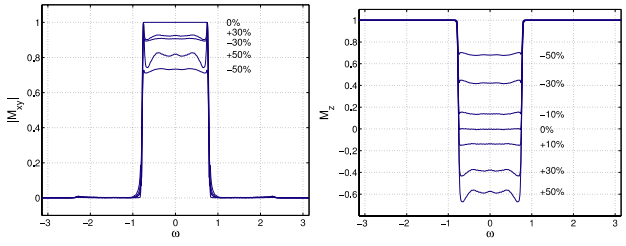

Fig. 10. Pulse profiles of quadratic-phase pulses generally deteriorate as $\tilde{B}_1$ is simply scaled to different flip angles. 0% denotes the original $\tilde{B}_1$ for a flip angle of 90°. Scaling the RF field by the indicated percentage alters the pulse profile as shown. For high profile quality, quadratic-phase pulses must be designed specifically for the target flip angle.

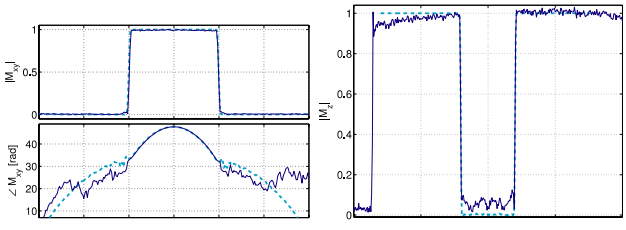

Fig. 11. Excitation (M_{xy}, left) and saturation (M_z, right) profiles obtained with a quadratic-phase Remez pulse, as simulated with a Runge–Kutta method (dashed) and measured experimentally using a water phantom (solid). In the saturation profile (right) a region outside of the phantom is included, reflecting the noise level present in the data set.

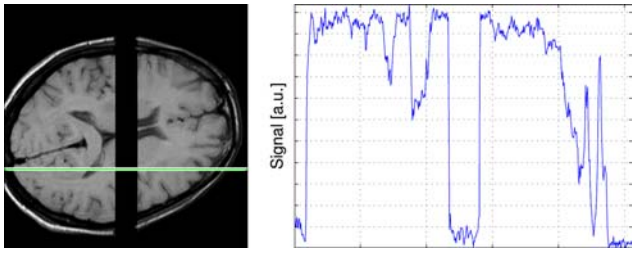

Fig. 12. Highly selective saturation by a quadratic-phase pulse exemplified in vivo on a healthy volunteer. A magnitude profile along the horizontal line on the left is plotted on the right.

(without JAVA) under a Linux operating system. The algorithm converged in the first stage after 18 iterations. While conceptually simpler than the complex Remez approach, the least-squares algorithm has not proven to be significantly faster than the latter. The main reason for this is the fine discretisation required for sufficient accuracy.

High time-bandwidth products rely on large filter lengths n and are thus practically limited by computing power. A time-bandwidth product in the range of 1000 (in radians) and above has been found to be readily feasible with current equipment. However, the application of such pulses in vivo may be restricted due to excessive power deposition.

6. Discussion and conclusion

In this work, we propose the use of the complex Remez algorithm for determining the complex filter coefficients in SLR design of quadratic-phase RF pulses. Although it is possible to obtain qualitatively similar results with the weighted least-squares approach, the key advantage of the Remez method is that it is straightforward to apply. Since it directly minimises the Chebyshev error norm, it obviates the need for a heuristic weighting function and directly achieves solutions with truly equi-ripple error function. While this work has focused on quadratic-phase low pass pulses, the general design method is applicable to pulses with arbitrary magnitude and phase response functions. Nevertheless, with any desired response function, it has been found that solutions with acceptable errors generally require proper choices of the design parameters.

This work also illustrates the specific benefits of quadratic phase modulation in a semi-analytic fashion (Section 2) and suggests parameter relations that may serve as guidelines for the design of these pulses (Section 3). In particular, a critical maximum value for the amount of quadratic phase k was obtained empirically. This limit and several further rules need to be observed in order to achieve markedly reduced $B_{1\,\max}$ without significant sacrifice in profile quality. It has been ob-

served that for parameters chosen within the suggested limits, the resulting error level will be similar to the error of the corresponding linear-phase pulse.

The profile quality of the quadratic-phase Remez pulses has been demonstrated by simulations and experiments. In vivo application has confirmed the usefulness of such pulses for a highly selective suppression of magnetisation and in vitro experiments have illustrated their applicability for both excitation and saturation. Nevertheless, in Fig. 11 some residual signal is still observed in the saturated band. The main reasons for the residual signal are noise and T_1 relaxation. The latter effect could be addressed by adjusting the flip angle for a given T_1 value. Some further deviation from perfect suppression may arise from slight mismatches between the analytical pulse description and the actual execution of the amplitude and frequency modulations by the MR system.

Numerous applications may benefit from the quadratic-phase pulses, which exhibit large bandwidth and high selectivity. Reduced field-of-view imaging and non-echo volume selection in spectroscopy are two applications already mentioned. Another prime application is the inversion of magnetisation. Currently, this task is often performed with adiabatic pulses. However, two factors favour the use of specifically designed quadratic phase pulses: for given time and $B_{1\,\max}$ restrictions better profiles can be achieved and the pulse energy will generally be lower than for adiabatic pulses. Such pulses will find use in many inversion-prepared sequences, in particular arterial spin labelling, where high selectivity is crucial.

While less intuitive, quadratic-phase RF pulses may indeed also be used for selective excitation, e.g., in 3D imaging [19,20]. Here, the additional phase encoding and Fourier reconstruction along the selection direction can make the quadratic phase variation negligible at the voxel scale. For common 2D imaging, quadratic phase modulation across a selected slice is usually a problem because it cannot be unwound with linear external gradients. Alternatively, phase compensation can be done by consecutive pulses with quadratic phase, where each pulse cancels the phase of the previous one [21]. Another way is to combine multiple pulse segments into a composite pulse [22], as originally done to create an adiabatic spin-echo pulse [23]. The downsides of these approaches are higher power deposition and longer pulse duration.

Finally, non-linear through-plane modulation may as well be exploited as a beneficial effect. Examples for such applications are spatial encoding by quadratic phase [24] and various methods for compensating B_0 inhomogeneity by quadratic- and tailored-phase RF pulses [25–27]. Requiring RF pulses with specific target phase responses, these methods will benefit from the flexibility and accuracy of complex Remez design.

Acknowledgments

The authors would like to thank Andreas Trabesinger for reviewing the manuscript. This work was supported by Philips Medical Systems (Best, NL); Eureka; KTI (Grant Nos. E!2061; 4178.1), INCA-MRI. Jeffrey Tsao is a recipient of a postdoctoral fellowship from the Canadian Institutes of Health Research (CIHR).

References

[1] D.W. Kunz, Use of frequency-modulated radio frequency pulses in MR imaging experiments, Magn. Reson. Med. 3 (3) (1986) 377–384.
[2] P. Le Roux, R.J. Gilles, G.C. McKinnon, P.G. Carlier, Optimized outer volume suppression for single-shot fast spin-echo cardiac imaging, J. Magn. Reson. Imaging 8 (5) (1998) 1022–1032.
[3] D.W. Kunz, H.H. Tuithof, J.H.M. Cuppen, Method and device for determining an NMR distribution in a region of a body, United States Patent 4,707,659 (1987).
[4] T.K.C. Tran, D.B. Vigneron, N. Sailasuta, J. Tropp, P. Le Roux, J. Kurhanewicz, S. Nelson, R. Hurd, Very selective suppression pulses for clinical MRSI studies of brain and prostate cancer, Magn. Reson. Med. 43 (1) (2000) 23–33.
[5] Y. Luo, R.A. de Graaf, L. DelaBarre, A. Tannus, M. Garwood, BISTRO: an outer-volume suppression method that tolerates RF field inhomogeneity, Magn. Reson. Med. 45 (6) (2001) 1095–1102.
[6] J.M. Pauly, D.G. Nishimura, A. Macovski, A k-space analysis of small-tip-angle excitation, J. Magn. Reson. 81 (1) (1989) 43–56.
[7] S.M. Conolly, D.G. Nishimura, A. Macovski, Optimal control solutions to the magnetic resonance selective excitation problem, IEEE T Med. Imaging MI-5 (2) (1986) 106–115.
[8] J. Mao, T.H. Mareci, K.N. Scott, E.R. Andrew, Selective inversion radio frequency pulses by optimal control, J. Magn. Reson. 70 (2) (1986) 310–318.
[9] H. Geen, S. Wimperis, R. Freeman, Band-selective pulses without phase distortion. A simulated annealing approach, J. Magn. Reson. 85 (3) (1989) 620–627.
[10] J.M. Pauly, P. Le Roux, D.G. Nishimura, A. Macovski, Parameter relations for the Shinnar–Le Roux selective excitation pulse design algorithm, IEEE T Med. Imaging 10 (1) (1991) 53–65.
[11] M. Shinnar, J.S. Leigh, The application of spinors to pulse synthesis and analysis, Magn. Reson. Med. 12 (1) (1989) 93–98.
[12] L.J. Karam, J.H. McClellan, Complex Chebyshev approximation for FIR filter design, IEEE T Circuits-II 42 (3) (1995) 207–216.
[13] L.J. Karam, J.H. McClellan, Chebyshev digital FIR filter design, Signal Process. 76 (1) (1999) 17–36.
[14] M. Shinnar, Reduced power selective excitation radio frequency pulses, Magn. Reson. Med. 32 (5) (1994) 658–660.
[15] A. Papoulis, Signal Analysis, McGraw-Hill, New York, 1977, Chapter 8.
[16] T.W. Parks, J.H. McClellan, Chebyshev approximation for nonrecusrive digital filters with linear phase, IEEE Trans. Circuit Theory CT 19 (2) (1972) 189–194.
[17] G.H. Golub, C.F. van Loan, Matrix Computations, third ed., The Johns Hopkins University Press, Baltimore, MD, 1996, Chapter 5.
[18] K.P. Pruessmann, M.A. Spiegel, G.R. Crelier, M. Stuber, M.B. Scheidegger, P. Boesiger, Fast simulation of MR-excitation considering flow and motion, Proc. Intl. Soc. Mag. Reson. Med. 5 (1997) 1537.
[19] J.M. Pauly, E.C. Wong, Non-linear phase RF pulses for reduced dynamic range in 3D RARE imaging, Proc. Intl. Soc. Mag. Reson. Med. 9 (2001) 688.

[20] L. DelaBarre, P.J. Bolan, M. Garwood, Improving dynamic range in 3D MRI with RF pulses producing quadratic phase, Proc. Intl. Soc. Mag. Reson. Med. 9 (2001) 690.
[21] D.W. Kunz, Frequency-modulated radiofrequency pulses in spin-echo and stimulated-echo experiments, Magn. Reson. Med. 4 (2) (1987) 129–136.
[22] K.E. Cano, M.A. Smith, A.J. Shaka, Adjustable, broadband, selective excitation with uniform phase, J. Magn. Reson. 155 (1) (2002) 131–139.
[23] S.M. Conolly, D.G. Nishimura, A. Macovski, A selective adiabatic spin-echo pulse, J. Magn. Reson. 83 (2) (1989) 324–334.
[24] J.G. Pipe, Spatial encoding and reconstruction in MRI with quadratic phase profiles, Magn. Reson. Med. 33 (1) (1995) 24–33.
[25] Z.H. Cho, Y.M. Ro, Reduction of susceptibility artifact in gradient-echo imaging, Magn. Reson. Med. 23 (1) (1992) 193–200.
[26] N. Chen, A.M. Wyrwicz, Removal of intravoxel dephasing artifact in gradient-echo images using a field-map based RF refocusing technique, Magn. Reson. Med. 42 (4) (1999) 807–812.
[27] A.W. Song, Single-shot EPI with signal recovery from the susceptibility-induced losses, Magn. Reson. Med. 46 (2) (2001) 407–411.